Geoderma 437 (2023) 116602

Contents lists available at ScienceDirect

Geoderma

journal homepage: www.elsevier.com/locate/geoderma

Silicon fractionations at the margin of a coastal wetland and its response to sea level rise

Xiangwei Zhao [a,b], Xiaodong Zhang [a,b,*], Zimin Li [c], Lukas Van Zwieten [d], Yidong Wang [e], Qian Hao [a,b], Yuqiu Wei [f], Xiangbin Ran [g], Xiaomin Yang [h], Zhaoliang Song [a,b], Hailong Wang [i,j]

[a] Institute of Surface-Earth System Science, School of Earth System Science, Tianjin University, Tianjin 300072, China
[b] Tianjin Key Laboratory of Earth Critical Zone Science and Sustainable Development in Bohai Rim, Tianjin University, Tianjin, China
[c] Earth and Life Institute, Soil Science, Université catholique de Louvain (UCLouvain), Croix du Sud 2, L7.05.10, 1348 Louvain-La-Neuve, Belgium
[d] Wollongbar Primary Industries Institute, NSW Department of Primary Industries, Australia
[e] Tianjin Key Laboratory of Water Resources and Environment, School of Geographic and Environmental Sciences, Tianjin Normal University, Tianjin, China
[f] Key Laboratory of Sustainable Development of Marine Fisheries, Ministry of Agriculture and Rural Affairs, Yellow Sea Fisheries Research Institute, Chinese Academy of Fishery Sciences, Qingdao, China
[g] Research Center for Marine Ecology, First Institute of Oceanography, Ministry of Natural Resources, Qingdao 266061, China
[h] Key Laboratory of Karst Georesources and Environment, Ministry of Education, College of Resources and Environmental Engineering, Guizhou University, Guiyang 550025, China
[i] School of Environmental and Chemical Engineering, Foshan University, Guangdong 528000, China
[j] Key Laboratory of Soil Contamination Bioremediation of Zhejiang Province, Zhejiang A & F University, Zhejiang 311300, China

ARTICLE INFO

Handling Editor: Matthew Tighe

Keywords:
Biogeochemical silicon cycling
Margin erosion
Sea level rise
Coastal wetland

ABSTRACT

Silicon (Si) and its biogeochemical cycling play an important role in maintaining the functions of terrestrial and marine ecosystems. However, the effects of sea level rise on the biogeochemical cycling of Si in coastal wetlands remain poorly understood. To explore this impact on biogeochemical Si cycling, we sampled a gradient from sediment to soil without the impact of tidal inundation in the Beidagang Wetland Nature Reserve, and then assayed non-crystalline Si (labile Si), including mobile Si ($CaCl_2$-Si), adsorbed Si (Acetic-Si), Si bound to soil organic matter (H_2O_2-Si), Si occluded in pedogenic oxides/hydroxide (Oxalate-Si), and amorphous Si (Na_2CO_3-Si) fractions. Analytical results showed that the content of $CaCl_2$-Si ranged from 13.0 to 53.3 mg kg^{-1} and the content of Acetic-Si ranged from 32.3 to 80.9 mg kg^{-1}, both of which were lower in sediments compared to soils. The content of H_2O_2-Si (84.1–160.1 mg kg^{-1}) and Oxalate-Si (306.6–655.1 mg kg^{-1}) in the soil profiles showed non-significant variations along the sampling slope. The Na_2CO_3-Si fraction accounted for 82%–90% of labile Si in soil and sediment, mainly being contributed from phytoliths or diatoms. Diatoms were only detected in sediment profiles. The storage of labile Si in sediment was significantly ($p = 0.0009$) lower than the storage in soil, suggesting that the coastal wetland ecosystems are an important source of Si to the estuary. With future sea level rise and increased margin erosion, the inter-transformation processes among different Si fractions would likely be weakened to increase dissolved Si for marine diatoms.

1. Introduction

Silicon (Si) is the second most abundant element on earth crust and its biogeochemical cycling is tightly linked to global carbon (C) cycling (Basile-Doelsch et al., 2005). When carbon dioxide (CO_2) reacts with silicate forming hydrogen carbonates (HCO_3^-) during weathering, Si enters the surrounding environment as silicic acid (Delvaux and Li, 2023). Si can also promote plant growth via alleviating abiotic and biotic stresses, thereby increasing the accumulation of biomass C (Ma et al., 2007; Liu et al., 2020). Components of dissolved Si (DSi) in terrestrial ecosystems can be transported to marine ecosystems by water movement, and then be taken up by diatoms (Conley et al., 2006). Indeed, there is growing evidence that diatoms play a key role in the biological C pump (Tréguer et al., 2018). Therefore, there is an urgent need to better understand the role of Si cycling in coastal wetlands.

Soils display a wide range of Si content ranging from < 1% up to >

* Corresponding author at: School of Earth System Science, Tianjin University, No. 92 Weijin Road Nankai District, Tianjin 300072, China.
E-mail address: xiaodongzhang521@tju.edu.cn (X. Zhang).

https://doi.org/10.1016/j.geoderma.2023.116602
Received 24 January 2023; Received in revised form 2 July 2023; Accepted 4 July 2023
Available online 7 July 2023

45%. The Si pool in soil comprises crystalline Si (stable Si), and non-crystalline Si (labile Si) (Sommer et al., 2006). Although there is a solid base of literature on stable Si in soils, little information is available on labile Si fractions, including mobile Si, adsorbed Si, Si bound to soil organic matter (SOM), Si occluded in pedogenic oxides/hydroxides, and amorphous Si (Sauer et al., 2006). Silicic acid is generally present as mobile Si in soils, ranging from 0.4 to 2000 μmol L^{-1}, and is largely dependent on parent material, adsorption, soil moisture, aggregation, and microbial activity (Conley et al., 2006; Cornelis et al., 2016; Li et al., 2022). Mobile Si can be adsorbed on the surfaces of the solid phases in soils, forming adsorbed Si (Georgiadis et al., 2013), which generally increases with the increasing specific surface area of the soil particles and is influenced by the soil composition and microbial activity (Gehlen and van Raaphorst, 2002; Yang et al., 2020a). Previous studies have also shown that silicic acid can be bound to SOM (Matichenkov and Bocharnikova, 2001; Sommer et al., 2006; Georgiadis et al., 2013), which was identified by Matichenkov and Snyder (1996) as complexes of organic compounds and Si in soil solution. The contents of pedogenic oxides and hydroxides in soils also play a key role in the adsorption, occlusion, and liberation of silicic acid (Opfergelt et al., 2009; Klotzbücher et al., 2020; Yang et al., 2020b). Amorphous Si originates from both biogenic and lithogenic sources, with biogenic sources generally dominating in most soil layers, including phytoliths, diatoms, and sponge spicules (Sartor et al., 2019; Puppe, 2020). Biogenic amorphous Si is thought to be the major source of DSi in soil solution, as its dissolution rate is 10^2–10^4 times greater than that of crystalline silicate minerals (Yang et al., 2020b; Fraysse et al., 2009). Furthermore, some of the silicic acid may transform to pedogenic amorphous Si via various processes such as precipitation and dehydration when saturation levels in the soil solution are reached (Dietzel, 2002). Although quantitative information exists on Si distribution in terrestrial soils (Georgiadis et al., 2014; Yang et al., 2020a; Hao et al., 2022), little information is available on different Si fractions in coastal wetlands (Georgiadis et al., 2017, Sartor et al., 2019).

Coastal wetland ecosystems, linking terrestrial and marine systems, have long been considered vulnerable to sea level rise (Struyf and Conley, 2009; Schuerch et al., 2018). Progressive inundation can reduce the contribution of plants to SOM and accelerate sloping margin erosion, thus speeding up the deterioration of coastal wetlands (Kirwan and Megonigal, 2013). Different degrees of sloping margin erosion have been reported for wetland-dominated coastal areas around the world (DeLaune and White, 2012; Sapkota and White, 2020). By combining spectroscopic and biogeochemical measurements, Steinmuller et al. (2020) illustrated that the continual erosion of soils at marsh edges had the potential to export labile C, N, and P into the ocean. However, the influence of coastal wetland erosion under sea level rise on soil Si fractions at different slope positions has not been reported.

In this study, we hypothesized that: (i) the pool sizes of the different Si fractions in coastal wetlands vary considerably; (ii) the distribution of the different Si fractions is related to both physicochemical properties of soil and to the degree of sea level rise; and (iii) these Si fractions play a key role in controlling the Si dynamics in coastal ecosystems. Therefore, sea level rise will affect the distribution, transformation, and storage of different Si fractions in coastal wetlands and thus regulate the global Si biogeochemical cycle. To test these hypotheses, a sequential chemical extraction method was used to assay Si fractionations along a gradient from sediment to soil without the impact of tidal inundation at the margin of a coastal wetland.

2. Materials and methods

2.1. Study area and sampling

The Beidagang Wetland Nature Reserve (BWNR) (38°36′–38°57′N, 117°11′–117°37′E), an internationally "important wetland", is located in the southeast of Tianjin, China (Fig. 1). It covers a total of 348.9 km^2, consisting of the core area, buffer zone, and experiment area. In this region, the climate is dominated by a northern subtropical monsoon, with a mean annual temperature of 11.3 °C (Yu et al., 2019). The mean annual potential evaporation is 1777 mm, the mean annual precipitation of which is 550 mm, with 70% of the rainfall concentrated between June to September (La et al., 2022). In the BWNR, *Phragmites australis* is the dominant species followed by *Suaeda salsa*, with the mixes of these two species being the third major vegetation type (Xia et al., 2021a).

Field survey and sampling were conducted at the core area of the BWNR in May 2021. The dominant vegetation at the sampling site was *P. australis*. Three independent replicate sampling transects were established from lower slope to upper slope, with five sampling points at each transect, at the margin of the BWNR (Fig. 1). The sediment is submerged by the water, while the soil is above the water level without being affected by the tidal inundation. Soil/Sediment samples were collected for five layers, including 0–5, 5–10, 10–20, 20–40, and 40–60 cm, giving a total of 75 samples. Depending on the waterlogging condition and slope, we defined sample sites C1 and C2 as the lower slope, which were submerged, while C4 and C5 were grouped as the upper slope, which were above tidal influence, and C3 became the middle

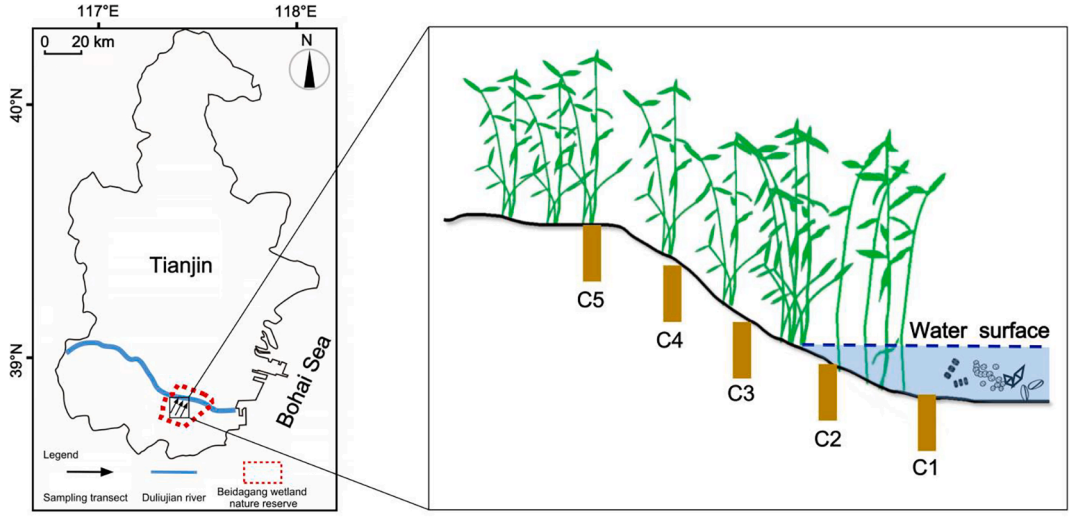

Fig. 1. Sampling location in the Beidagang Wetland Nature Reserve of Tianjin, China. Three independent replicate sampling transects were established from lower slope to upper slope at the margin of the coastal wetland. The figure on the right shows that one typical transect with five sampling points (C1–C5) along the slope.

slope. All samples were individually air-dried and sieved through 2 mm and a portion of the sieved sample through 0.15 mm after removal of visible root residues and organic debris. In addition, the aboveground biomass of *P. australis* was collected within a 1 m × 1 m sampling square at each of C1–C5 from each transect. The collected plant samples were rinsed with distilled water, dried at 65 °C to a constant weight, and ground prior to analysis.

2.2. Sample analyses

Samples pH (soil:water suspension = 1:2.5 (w/v)) and electrical conductivity (EC) (soil:water suspension = 1:5 (w/v)) were determined using a pH/conductivity meter. Bulk density (BD, g cm^{-3}) was measured by the cutting ring method (100 cm^3) and weighing. As some profiles could not be collected by the ring knife, soil organic carbon (SOC) was used to calculate the BD, based on an empirical formula (Xiao, et al., 2019). Particle size distribution of the soils was measured using a laser particle size analyzer (Mastersizer 3000, Malvern, UK). The contents of total organic C in samples were determined using the potassium dichromate method (Walkley and Black, 1934; Lu, 2000). Approximately 30 mg of soil samples were fused with Li-metaborate at 950 °C, dissolved in dilute nitric acid, for analyzing total elements (Si, P, Al, and Fe) using an ultraviolet–visible spectrophotometer (UV-1800, Shimadzu, Japan). Total Si content in plants was measured by the Li-metaborate fusion and molybdenum blue colorimetric method (Lu 2000). Each analysis of soil and plant samples had three replicates.

A sequential chemical extraction method was used to divide the labile Si into five sub-fractions, including mobile Si ($CaCl_2$-Si), adsorbed Si (Acetic-Si), Si bound to SOM (H_2O_2-Si), Si occluded in pedogenic oxides/hydroxide (Oxalate-Si), and amorphous Si (Na_2CO_3-Si) (Georgiadis et al., 2013, 2017; Yang et al., 2020b). The detailed methods for the extraction of each Si fraction are shown in Table S1. The Si contents in all extractions were analyzed by the molybdenum blue colorimetric method using an ultraviolet–visible spectrophotometer (Lu, 2000). Si in primary and secondary minerals in the soils was calculated as the difference between total Si and labile Si represented by the sum of the five sub-fractions. To extract biogenic amorphous Si particles from soil samples, a wet oxidation and heavy liquid suspension method was used (Zuo et al., 2014; Song et al., 2022). The isolate extracted from soils was digested using the Walkley-Black method to make sure that any organic matter outside the biogenic amorphous Si particles was completely removed (Walkley and Black, 1934; Li et al., 2013). Furthermore, the biogenic amorphous Si particles were oven-dried to a constant mass at 60 °C for 24 h. A scanning electron microscope (SEM, Sigma500, ZEISS, Germany) equipped with an energy dispersive spectrometer (EDS, X-Max^N 80, Oxford, UK) was used to characterize the morphological features and surface chemical composition of the biogenic amorphous Si particles.

2.3. Data calculation

In our study, the storage (ST) of the different Si fractions in soil profiles was calculated as follow (Yang et al., 2020a):

$$ST = \left(\sum_{i=1}^{n} D_i \times BD_i \times C_i \right) \div 10$$

where ST (t Si ha^{-1}) is the storage value for the extracted Si fraction in soils; i ($i = 1, 2, 3, 4, 5$) is the soil profile horizon from surface to bottom soil (i.e., 0–5, 5–10, 10–20, 20–40 and 40–60 cm); D_i (cm) is the thickness of the i layer; BD_i (g cm^{-3}) is the bulk density of the i layer; and C_i (g kg^{-1}) is the content of Si extracted in each fraction in the soil horizon.

It was common practice to estimate the BD from an empirical relationship between the SOC content and the BD (Xiao et al., 2019; Xia et al., 2022). Where some soil profiles could not be collected by the ring knife, the SOC for each layer was used to calculate the BD based on the following equation (Xiao et al., 2019):

$$BD = 0.8572 \times e^{-0.0331 \times SOC} + 0.7446 \times e^{-0.0027 \times SOC}$$

where BD is bulk density (g cm^{-3}), and SOC is soil organic carbon (g kg^{-1}). A linear regression analysis of actual measured BD and empirically estimated BD was performed with an $R^2 = 0.7399$ and $p < 0.0001$, indicating that our estimated BD are acceptable (Fig. S1).

2.4. Statistical analysis

Data were tested for homogeneity and normality before the analysis. The results for each site were the mean value and the standard deviation of the three replicates. One-way analysis of variance (ANOVA) with Tukey's test was used to compare the significant differences ($p < 0.05$) in the content or storage of different Si fractions among sampling sites. Pearson correlation analysis was performed to reveal the correlation between the content of different Si fractions and soil physicochemical properties. In addition, redundancy analysis (RDA) was carried out to assess the variance in different Si fractions explained by soil physicochemical properties. Pearson correlation analysis and RDA were performed by SPSS ver.21.0 and R statistic software, respectively.

3. Results

3.1. Changes in soil physicochemical properties

Soil pH, ranging from 8.07 to 9.17, generally increased with depth but showed no statistical difference along the sampling slope (C1–C5). In contrast, soil EC was influenced by slope location, with sites in the tidal zone having higher EC than those above the tidal influence. SOC contents (4.0–23.9 g kg^{-1}) showed a decreasing trend with increasing depth and gradually increased from sampling point C1 to C5 in the surface soil (0–5 cm). Total P contents ranged from 0.52 to 0.87 g kg^{-1} and were generally higher in the upper layers than those in the lower layer (Table 1). Particle size distribution of soils varied from 12.8% to 17.4% for clay, 82.1% to 85.5% for silt, and 0 to 2.2% for sand. Other soil properties, such as total Fe and Al contents, did not show statistical differences among different depths or locations along the slope (Table S2).

3.2. Distribution of different Si fractions

The content of stable Si (mainly bound to primary and secondary silicates) in soils ranged from 227.7 to 293.7 g kg^{-1}, accounting for 97%–98% of the total Si. The largest content of stable Si was detected in the 20–30 cm soil layer of C3, coinciding with a lower level of Na_2CO_3-Si. The $CaCl_2$-Si and Acetic-Si contents tended to decrease with soil depth and ranged from 13.0 to 53.3 mg kg^{-1} and from 32.3 to 80.9 mg kg^{-1}, making up 0.3%–0.6% and 0.7%–1.1% of the labile Si, respectively. The contents of $CaCl_2$-Si and Acetic-Si fractions were lower in submerged soils than in the other soils. The H_2O_2-Si fraction constituted between 1.6% and 3.1% of the labile Si, with the content ranging from 84.1 to 160.1 mg kg^{-1}. The content of Si occluded in pedogenic oxides/hydroxides (Oxalate-Si) ranged from 306.6 to 655.6 mg kg^{-1}, or 6.7% to 14.3% of the labile Si, and tended to increase with depth in all soil profiles. The contents of H_2O_2-Si and Oxalate-Si in the upper layer were similar across all sampling sites. The Na_2CO_3-Si (3.2–6.9 g kg^{-1}) was the most dominant labile Si fraction, comprising 82%–90% of the labile Si, corresponding to 1.3%–2.3% of the total Si. The contents of Na_2CO_3-Si and labile Si had a similar decreasing trend with increasing soil depth. The content of Na_2CO_3-Si in the surface layers increased as the sampling location moved away from the tidal influence (Figs. 2 and 3).

Table 1
Selected soil physicochemical characteristics of the studied soil profiles.

Site	Depth (cm)	pH	EC (μS cm^{-1})	SOC (g kg^{-1})	Total Si (g kg^{-1})	Total P (g kg^{-1})
C1	0–5	8.53	1291	10.47	249.95	0.70
		(0.13)	(329)	(1.35)	(12.86)	(0.04)
	5–10	8.75	954 (62)	6.56	256.48	0.68
		(0.12)		(0.23)	(8.05)	(0.06)
	10–20	8.89	768	5.59	257.28	0.66
		(0.10)	(126)	(0.66)	(12.96)	(0.02)
	20–40	8.96	562	4.77	252.83	0.68
		(0.13)	(139)	(0.30)	(8.43)	(0.04)
	40–60	9.06	554	4.56	258.33	0.65
		(0.15)	(140)	(0.36)	(30.80)	(0.02)
C2	0–5	8.49	1212	14.91	256.70	0.72
		(0.15)	(184)	(2.60)	(4.29)	(0.01)
	5–10	8.58	733	8.45	254.95	0.68
		(0.27)	(128)	(1.35)	(2.06)	(0.01)
	10–20	8.74	735	5.97	258.40	0.67
		(0.17)	(138)	(0.78)	(3.98)	(0.03)
	20–40	8.74	523 (91)	5.38	252.45	0.66
		(0.13)		(0.42)	(9.21)	(0.01)
	40–60	8.93	632	4.42	257.54	0.67
		(0.25)	(109)	(0.39)	(19.28)	(0.02)
C3	0–5	8.41	660	14.94	264.81	0.75
		(0.22)	(140)	(4.03)	(12.23)	(0.03)
	5–10	8.83	559	7.43	242.37	0.72
		(0.06)	(119)	(2.55)	(1.89)	(0.06)
	10–20	8.57	551	5.44	263.21	0.71
		(0.15)	(128)	(1.40)	(1.73)	(0.03)
	20–40	8.89	574	5.27	270.64	0.68
		(0.17)	(126)	(0.79)	(11.21)	(0.02)
	40–60	9.01	531 (90)	4.81	255.14	0.60
		(0.15)		(1.05)	(26.39)	(0.07)
C4	0–5	8.33	732 (97)	19.68	272.15	0.82
		(0.21)		(3.86)	(12.32)	(0.05)
	5–10	8.34	610	9.59	267.75	0.73
		(0.27)	(106)	(2.54)	(9.90)	(0.07)
	10–20	8.62	589 (50)	5.33	262.85	0.69
		(0.15)		(1.26)	(7.27)	(0.03)
	20–40	8.75	642 (62)	4.80	261.71	0.72
		(0.11)		(0.32)	(4.24)	(0.02)
	40–60	8.85	476 (93)	4.91	267.37	0.70
		(0.16)		(0.70)	(13.32)	(0.06)
C5	0–5	8.19	506 (62)	15.29	271.61	0.78
		(0.13)		(3.59)	(10.12)	(0.07)
	5–10	8.47	343 (55)	10.08	271.61	0.71
		(0.13)		(1.77)	(6.97)	(0.10)
	10–20	8.37	310 (58)	6.54	263.03	0.69
		(0.15)		(0.32)	(8.13)	(0.08)
	20–40	8.75	335 (94)	4.92	269.25	0.74
		(0.07)		(0.15)	(12.66)	(0.04)
	40–60	8.77	316 (97)	5.24	261.56	0.74
		(0.20)		(0.78)	(7.10)	(0.03)

All data are presented as means with standard deviation (in brackets).

3.3. Storage of different Si fractions

The storage of $CaCl_2$-Si and Acetic-Si represented a very small proportion of Si pool, ranging from 0.13 to 0.23 t ha^{-1} and from 0.35 to 0.47 t ha^{-1} in the top 60 cm soil layers, respectively. The storage of these two Si fractions was significantly lower ($p = 0.0015$ and $p = 0.0008$) in sediments than in non-submerged soils. The storage of H_2O_2-Si ranged from 0.93 to 1.22 t ha^{-1}, while Oxalate-Si ranged from 4.11 to 5.11 t ha^{-1} with no significant difference among sampling sites for the storage of the two Si fractions ($p = 0.053$ and $p = 0.343$). The dominant fraction, Na_2CO_3-Si, ranged from 29.37 to 41.09 t ha^{-1}, with significant differences ($p = 0.0009$) between sediments and soils (Fig. 4).

3.4. Forms of biogenic amorphous Si particles

SEM revealed the presence of different forms of biogenic amorphous Si particles (Fig. 5), with the phytoliths as the dominant form. The main phytolith types were elongated, rondel, saddle, bilobate and triangular prismatic. In contrast to the relatively smooth surface of phytoliths in the upper soil layers, large portions of the phytoliths' surfaces have been corroded in the lowermost horizons (Fig. S2). Diatoms were found mostly at C1 and C2. SEM-EDS analysis showed that the diatoms generally had higher Si:C atomic ratios than the phytoliths (Fig. 5g–i).

3.5. Correlations among soil properties and Si fractions

Pearson's correlations showed a significant and strong positive relationship ($r = 0.87$, $p = 6.2e{-}21$) between the $CaCl_2$-Si and Acetic-Si fractions. A positive correlation was found between Na_2CO_3-Si and $CaCl_2$-Si. The soil pH was negatively correlated with the Na_2CO_3-Si fraction ($r = -0.58$, $p = 3.4e{-}7$), but positively correlated with the Oxalate-Si fraction ($r = 0.45$, $p = 1.5e{-}4.3$). There was a correlation between SOC and different Si fractions. Total P was significantly correlated with three forms of Si ($CaCl_2$-Si, Acetic-Si, and Na_2CO_3-Si). In addition, there was a significant correlation between the Oxalate-Si and total Al ($r = 0.38$, $p = 0.0018$), whereas the Oxalate-Si did not show any correlation with the total Fe, suggesting that more Si was mainly bound to or co-precipitated with Al oxides/hydroxides rather than Fe oxides/hydroxides (Fig. 6). RDA combined with Pearson's correlations showed that soil physicochemical properties and the content of different Si fractions had apparent discrepancies in different sampling groups. The soil pH, SOC and total P were the primary soil properties controlling different Si fractions in the studied areas (Fig. 7).

4. Discussion

4.1. Factors influencing the distribution of different Si fraction quantities

Soil pH is an important factor affecting soil Si bioavailability, and generally exhibits a positive correlation with the $CaCl_2$-Si fraction (Georgiadis et al., 2014; Yang et al., 2020a; Wu et al., 2022), particularly in acidic to neutral soils (Yang et al., 2021). However, no positive correlation between soil pH and $CaCl_2$-Si was detected in the soils of the BWNR. This was likely due to the high pH of these soils which ranged from 8.07 to 9.17 (Table 1). The effect of soil pH on the $CaCl_2$-Si fraction is also influenced by soil texture and SOC (Struyf et al., 2010; Imtiaz et al., 2016). In particular, a high pH condition generally enhances soil aggregation, leading to decrease Si bioavailability and DSi release (Li et al., 2023). The Na_2CO_3-Si fraction includes both biogenic amorphous Si (e.g., phytolith, diatom, etc.) and pedogenic Si (e.g., allophanes), which was the main fraction contributing to the labile Si pool (Sauer et al., 2006; Cornelis et al., 2016; Li et al., 2022). In this study, we found that phytoliths were the major source of biogenic amorphous Si (Fig. 5). Fraysse et al. (2009) have demonstrated that the dissolution rate of phytoliths increased linearly with increasing pH. Our observations supported this as Na_2CO_3-Si content decreased with depth in each soil profile, concomitant to increasing alkalinity (Table 1 and Fig. 2).

Coastal wetland soils generally accumulate more organic matter than terrestrial soils (Xia et al., 2021b). On the one hand, SOM provides more attachment points for the adsorption of monosilicic acid (Yang et al., 2020b). On the other hand, the decomposition of SOM generates organic acids and reducing conditions contributing to the release of Si associated with Fe and Mn oxides (Siipola et al., 2016; Georgiadis et al., 2017; Klotzbücher et al., 2020). Thus, SOC was positively correlated with both $CaCl_2$-Si and Acetic-Si (Fig. 6), a result supported by Wu et al. (2022). In forest soils, the vertical distribution of the H_2O_2-Si fraction was positively correlated with SOC (Yang et al., 2020a). However, coastal wetland soils of our study area exhibited no positive correlation between the H_2O_2-Si fraction and SOC (Fig. 6), possibly because treatment with hot H_2O_2 extractant led to the release of some Si from clay minerals, pedogenic oxides and bio-opal (Georgiadis et al., 2013). Previous studies also reported that hot H_2O_2 reacted with clay minerals, especially smectite, which could weaken the positive correlations between H_2O_2-Si

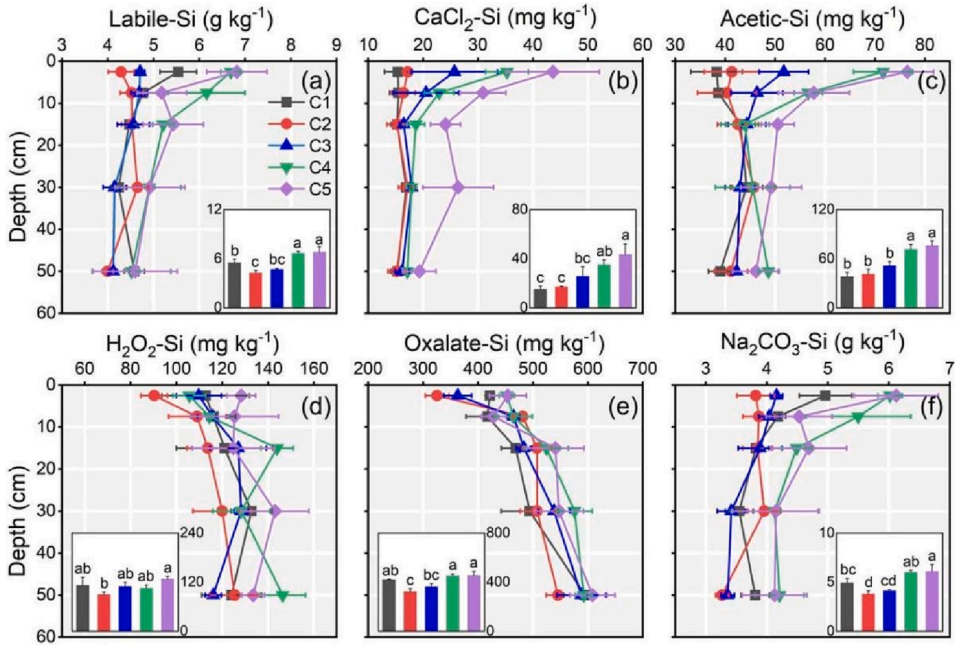

Fig. 2. Contents of Si fractions within the 0–60 cm soil layer of the studied area. The inset shows the different Si fraction contents changing within the surface layer (0–5 cm) at different slope points.

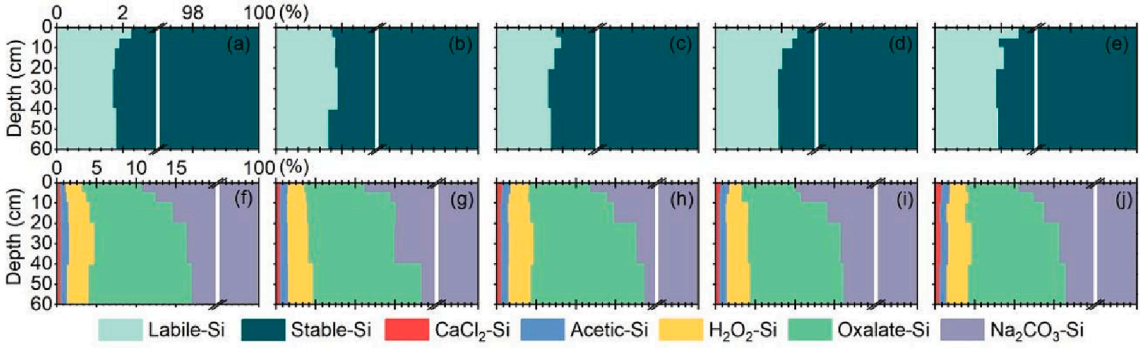

Fig. 3. Vertical percentage distribution of the labile Si and stable Si fractions of the total Si (a-e) and the $CaCl_2$-Si, Acetic-Si, and H_2O_2-Si, Oxalate-Si and Na_2CO_3-Si fractions in the labile Sifraction (f-j) within the 0–60 cm soil layer along different slope points.

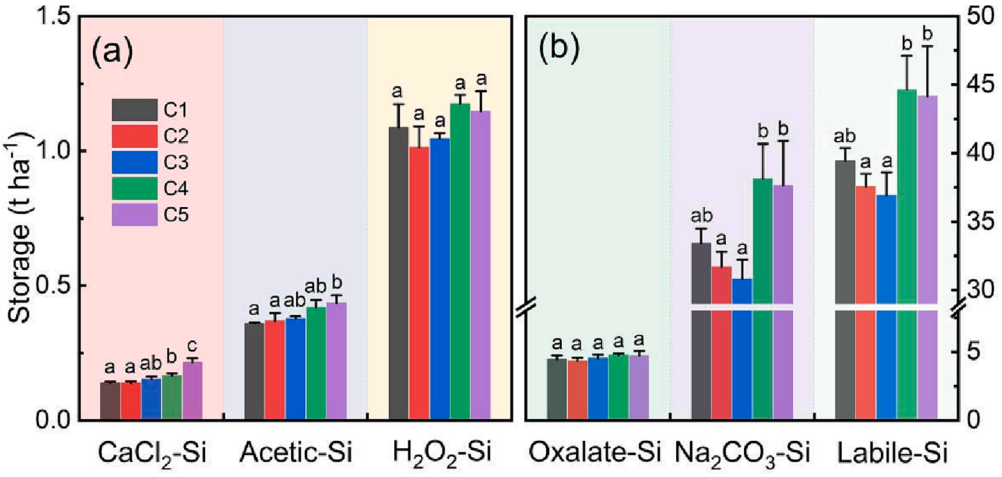

Fig. 4. Storage of $CaCl_2$-Si, Acetic-Si, H_2O_2-Si, Oxalate-Si, Na_2CO_3-Si, and labile-Si fractions within the 0–60 cm soil layer along the position slopes. Different letters indicate significant differences among the different Si fractions at $p < 0.05$.

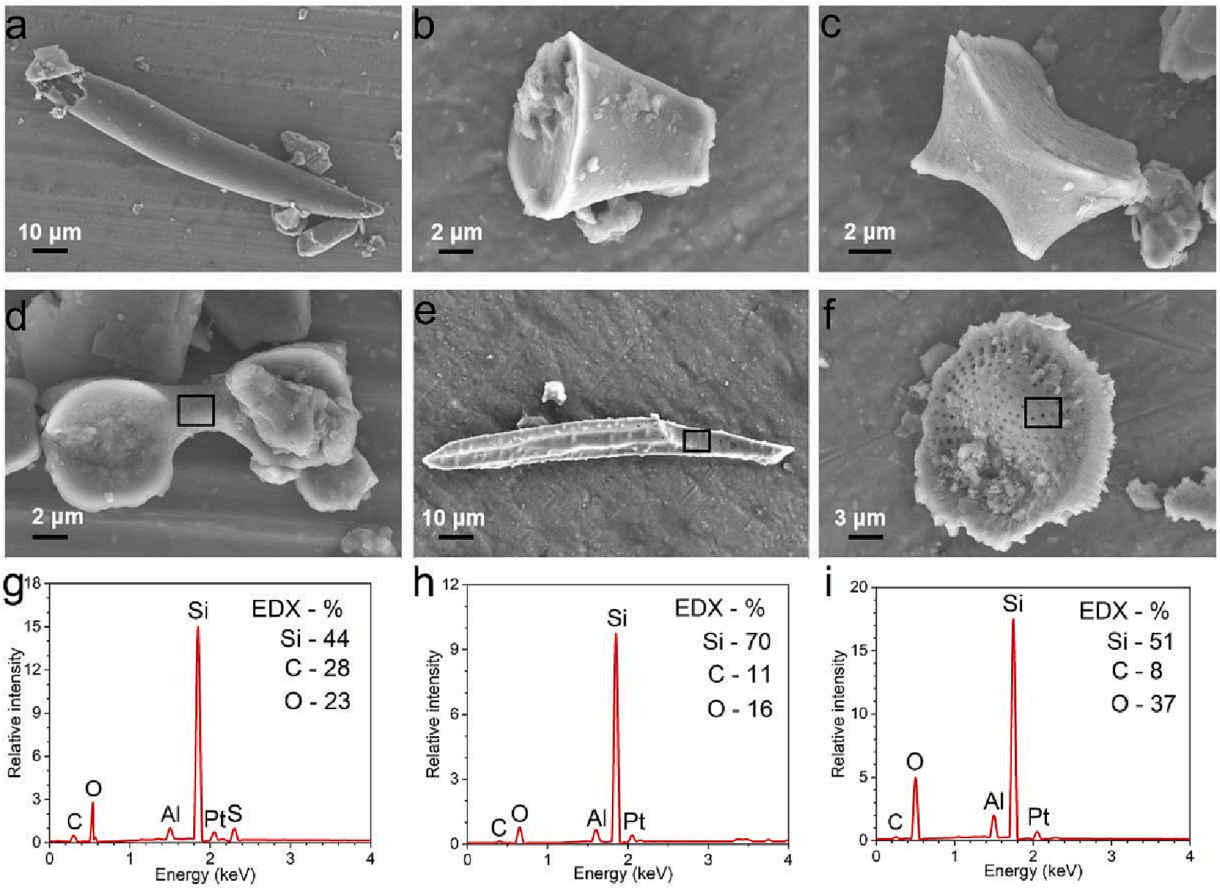

Fig. 5. SEM-micrographs of different types of biogenic amorphous Si particles (a) elongated, (b) rondel, (c) saddle, (d) bilobate, (e) triangular prismatic phytoliths and (f) diatom (*Coscinodiscus* spp.) and the results of corresponding element mapping (g–h) corresponding to d–f.

and SOC (Georgiadis et al., 2014, 2017). Furthermore, charcoal may represent an additional source of H_2O_2-Si, but the charcoal will not be completely oxidized by the concentrated H_2O_2, resulting in a portion of H_2O_2-Si that may not be released from the soils (Georgiadis et al., 2017). We found a close positive correlation ($r = 0.64$, $p = 6.8e{-}9$) between SOC and Na_2CO_3-Si (Fig. 6). As important contributors to Na_2CO_3-Si, phytoliths and diatoms can sequester organic C during their formation or growth (Song et al., 2016; Tréguer et al., 2021). Generally, the organic C occluded by both phytoliths and diatom frustules may be accumulated in soil and sediment over a long time period (hundreds to thousands of years) due to the protection of siliceous shells (Parr and Sullivan, 2005; Zhang et al., 2020; Song et al., 2022). The contents of Na_2CO_3-Si and SOC followed similar trends down the soil profiles supporting the correlation between these factors (Table 1 and Fig. 2). However, it was still not clear to what extent, and indeed how the SOC fraction, which was independent from biogenic amorphous Si particles, affected the organic C occluded in phytoliths and diatom frustules.

The relationship between soil Si availability and other nutrients were mainly manifested in the interaction between Si and P (Liang et al., 2015). Phosphate was considered in the extraction medium for assaying adsorbed Si in soils and sediments, due to anion exchange with silicate ions (Andreola et al., 2004; Georgiadis et al., 2013). The positive correlation between total P and labile Si implied the occurrence of exchange reactions between phosphate and silicate ions in the studied soils (Fig. 6). Similar studies have shown that the contents of adsorbed Si extracted by phosphate were generally high due to the interactions of phosphate with partial clay minerals (Andreola et al., 2004). For this reason, phosphate was not considered as a good extractant for adsorbed silicic acid. However, no correlation was found between Oxalate-Si and total P in the current study (Fig. 6). Phosphorus is an essential mineral element for plant growth and has been shown to be a common limiting nutrient for many coastal wetland ecosystems (Wang et al., 2018). The total P content (mean = 0.70 g kg^{-1}) in the studied soils was higher than the national average (0.50 g kg^{-1}) (Tian et al., 2010). Li et al. (2020) studied the impact of combined Si-P fertilization on the production of phytoliths by plants and found that it could significantly increase phytolith contents, which in turn lifted the content of biogenic amorphous Si in soil and sediment. Therefore, in coastal wetlands with sufficient $CaCl_2$-Si contents, increasing total P concentration in soil can promote the formation of phytoliths in plant tissues, subsequently increasing the content of Na_2CO_3-Si in associated soils, which was supported by the positive correlation between Na_2CO_3-Si contents and total P in the studied soils (Fig. 6).

4.2. Sources and transformation processes of amorphous Si

The dominant labile Si fraction was Na_2CO_3-Si (Figs. 2 and 3), consisting of amorphous Si from both biogenic and lithogenic sources (Cornelis et al., 2011). In terrestrial soils, phytoliths produced by higher plants were the main component of biogenic amorphous Si, with Si-containing bacteria and fungi making a minor contribution (Street-Perrott and Barker, 2008). In marine systems, biogenic amorphous Si was generally considered to be derived from diatoms, with smaller contributions from dinoflagellates, sponges and radiolaria (Nelson et al., 1995). In land-sea interface ecosystems, biogenic amorphous Si can be both land- and ocean-derived. Our study revealed that phytoliths dominated all soil profiles, while diatoms were only observed in sediments (Fig. 5). The absence or minimal content of biogenic amorphous Si particles, along with the high Na_2CO_3-Si content, suggested that other mechanisms were involved in the formation of amorphous Si.

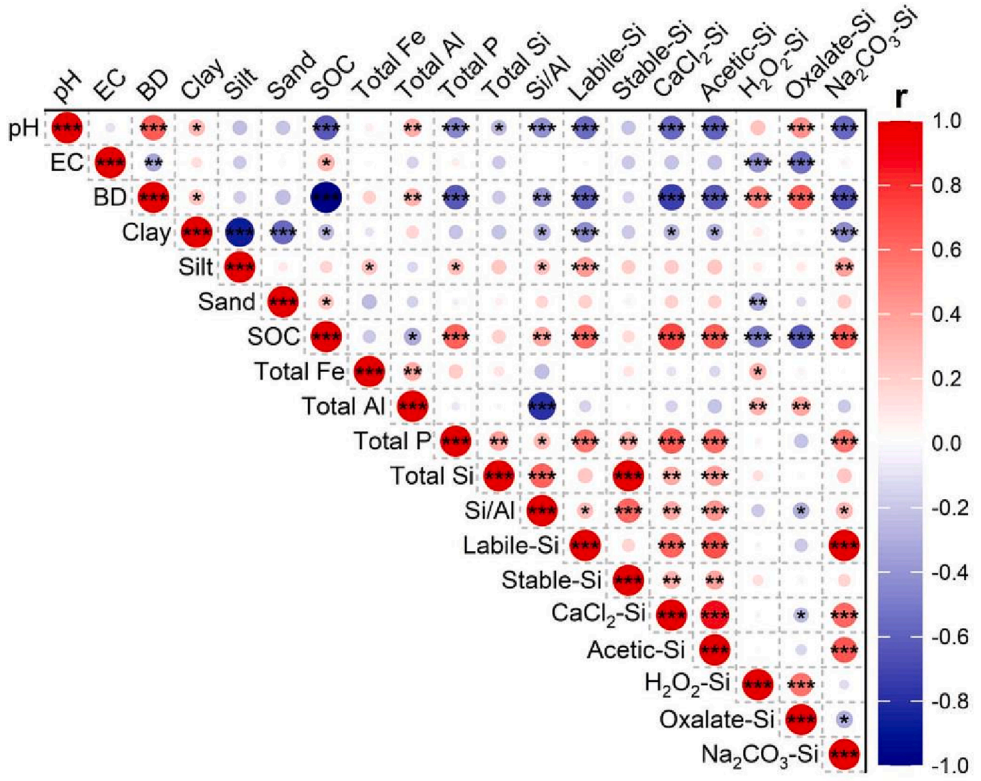

Fig. 6. Pearson correlations between different Si fractions and soil properties. * Correlation is significant at $p < 0.05$; ** Correlation is significant at $p < 0.01$; *** Correlation is significant at $p < 0.001$.

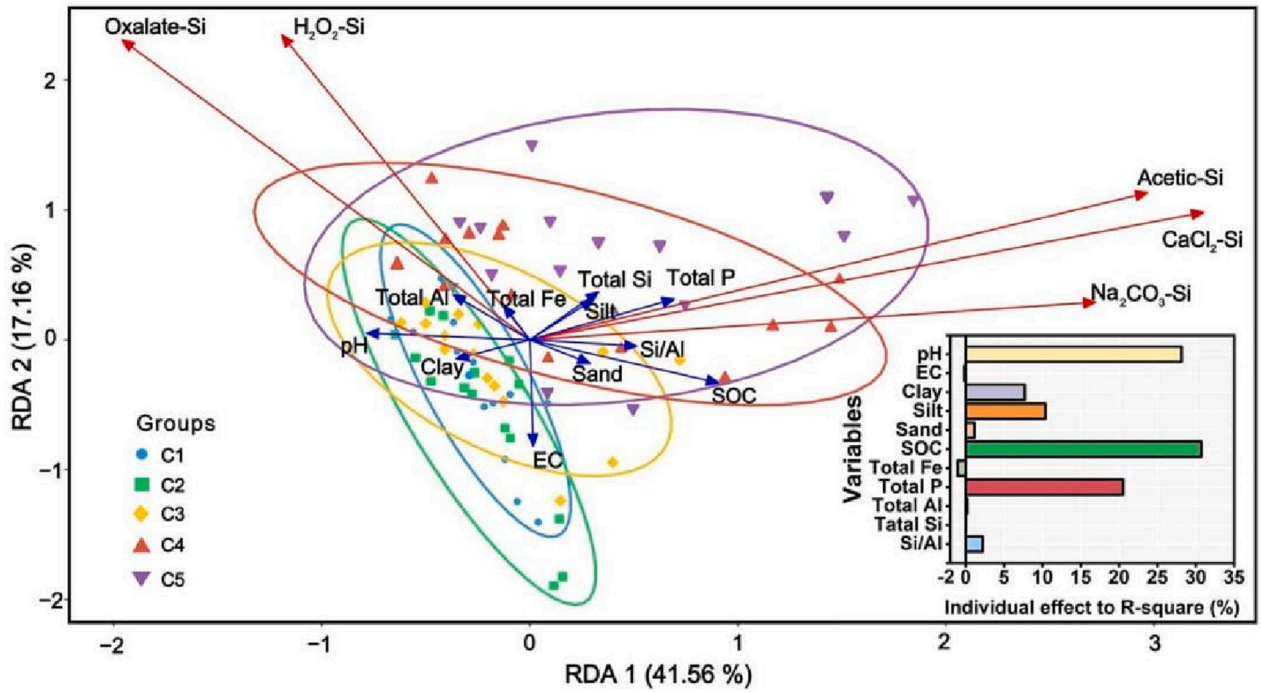

Fig. 7. Redundancy analysis of different Si fractions and soil physicochemical properties at different slope positions. The inset shows the relative importance of different soil properties in regulating different Si fractions.

Mineralogic amorphous Si can precipitate when soil conditions favor the increase in dissolved Si levels, forming coatings on mineral grains or mixtures with crystalline substances (Saccone et al., 2007). Previous research showed that hypersaline tidal flats driven by high evaporation were favorable for pedogenic amorphous Si precipitation (Sartor et al., 2019).

Traditionally, the dissolution of biogenic amorphous Si conformed to first order kinetics, and the rate increased linearly with the degree of

undersaturation in the solution (Gallinari, et al., 2002). However, due to a variety of other factors (e.g., pH, reactive surface area, electrolyte composition of the solution) that could potentially affect the dissolution of amorphous Si, the dissolution rate of biogenic amorphous Si was not a simple linear relationship (Van Cappellen and Qiu, 1997). The pH dependence of the dissolution kinetics of phytoliths was investigated using a flow through reactor experiment, indicating that the dissolution rate of phytoliths lay between those of quartz and vitreous silica and exhibit similar dependence at pH between 4 and 12 (Fraysse et al., 2009). In addition, the rate of release of silicic acid from biogenic amorphous Si was proportional to the amount of reactive surface area exposed by the skeletal particles at a given degree of undersaturation (Hurd and Birdwhistell, 1983). Furthermore, Dove and Elston (1992) found that surface complexes involving adsorbed alkali cations, such as ≡SiONa, may accelerate the dissolution of biogenic amorphous Si, while other adsorbed cations (e.g., Al^{3+}) may reduce the surface reactivity of silica (Dixit et al., 2001). However, we found an insignificant correlation between the content of Al and Na_2CO_3-Si (Fig. 6), as Al may be present in an anionic form ($Al(OH)_4^-$) and thus ineffective for phytolith preservation in alkaline soils (Nguyen et al., 2019). As soil biogenic amorphous Si particles extracted by heavy liquid flotation were concentrated in the surface soil horizon, the dissolution of "fresh" biogenic amorphous Si particles was the main source of plant-available Si ($CaCl_2$-Si). There were "old" biogenic amorphous Si particles in the deep soil layer (Fig. S2), which underwent a prolonged weathering process with observable pores and pit holes on the surface (Van Cappellen and Qiu, 1997; de Tombeur et al., 2020), further supporting the notion of phytolith dissolution in the coastal soil/sediment system.

4.3. Implications of sea level rise for biogeochemical Si cycling

Different Si components inter-transformed with each other, which was an important process of Si biogeochemical cycle in coastal wetland ecosystems. The transformation relationships among these Si pools were extremely significant on the upper slope without tidal influence (Fig. 8). Although our study showed that the $CaCl_2$-Si fraction accounted for a minor component of the labile Si pool, it was also the most available being directly absorbed by plant roots (Song et al., 2014). The other four labile Si fractions had potential inter-transformation processes with $CaCl_2$-Si, indicating that the reduction in the $CaCl_2$-Si fraction as plant uptake could promote the conversion of the other non-crystalline Si fractions into silicic acid, thus counteracting the losses of $CaCl_2$-Si (White et al., 2012; Song et al., 2018). Additionally, the pedogenic oxides and hydroxides could also regulate the Si supplies through adsorption and desorption processes (Georgiadis et al., 2013; Li and Delvaux, 2019; Li et al., 2023). Therefore, the $CaCl_2$-Si fraction may act as a pivotal driver of the biogeochemical cycling of Si in coastal wetland ecosystems. Weathering caused the hydrolyzation of stable Si, forming DSi in soil solution (Sommer et al., 2006; Cornelis et al., 2016). Most crystalline Si had a slow weathering rate, and the contribution of this fraction to Si bioavailability was small over short time scales (Dietzel, 2000). The Na_2CO_3-Si such as phytolith and diatom shells was the largest components of the labile Si fraction, with the dissolution rate being 4 orders of magnitude higher than for the primary and secondary silicates (Fraysse et al., 2009). This means that the pool size of the water-soluble Si mainly depends on the dissolution of biogenic amorphous Si (Yang et al., 2019). Additionally, there was a rapid turnover of phytogenic Si through litter fall or root decomposition of *P. australis*, thus contributing to the accumulation of phytoliths in soil (Fig. 8).

The margin erosion under sea level rise of coastal wetlands may weaken the inter-transformation among different Si fractions at the submerged sites (Fig. 8). Affected by rainfall and occasional tidal inundation, amorphous Si (fresh phytoliths) may be lost (Vander Linden et al., 2021). We suspected that this may be the reason why the Na_2CO_3-Si content at the middle slope was lower ($p = 0.004$) than that at the upper slope (Fig. 8). The phytoliths lost from the middle slope will then contribute to the Na_2CO_3-Si pool in the inundated sediments. However, there were two possible fates for the amorphous Si deposited in the sediments at the lower slope. On the one hand, the amorphous Si transported and became incorporated into the sediment, becoming

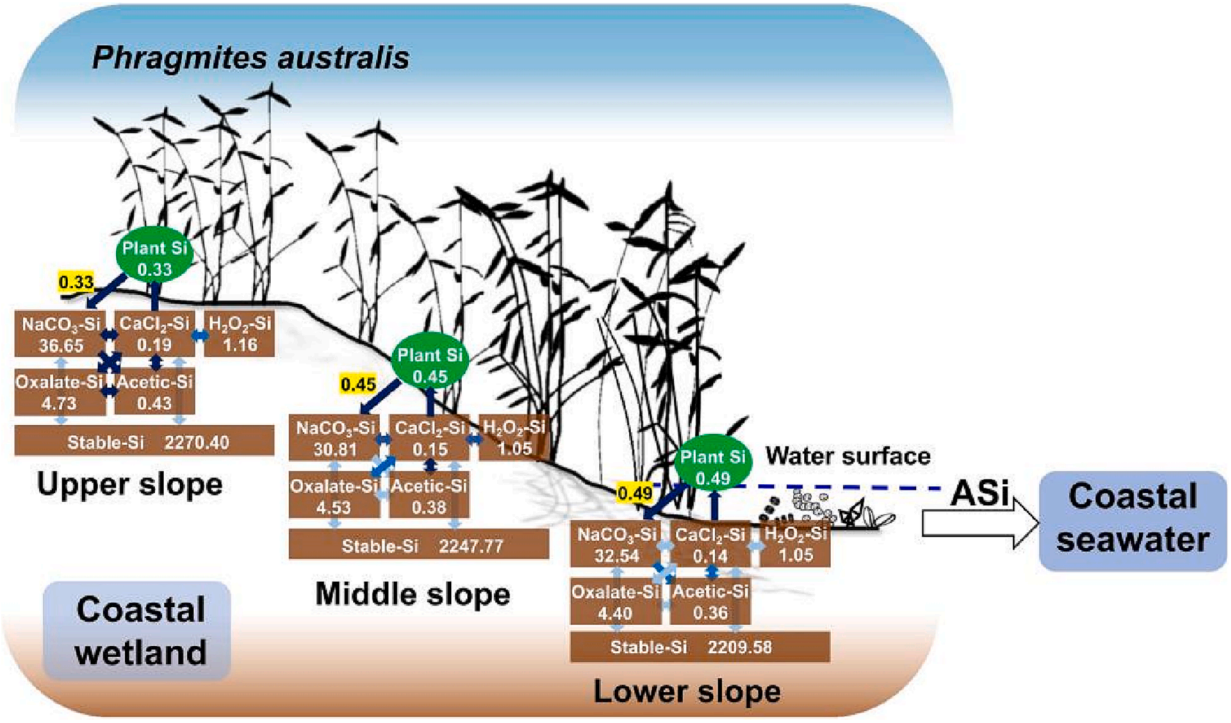

Fig. 8. A conceptual model of Si conversion between the different Si pools (t Si ha^{-1}) along the slope positions at the margin of the coastal wetland. The inter-transformation between different Si fractions is indicated by the three tones of blue arrows (light, insignificant; normal, $p < 0.05$; dark, $p < 0.01$). (For interpretation of the references to colour in this figure legend, the reader is referred to the web version of this article.)

buried over time. On the other hand, amorphous Si can be physically transported further into the bay and subsequently dissolved. In either case, both of these processes could result in the loss of stored amorphous Si at the lower slope, providing DSi for the estuary. Generally, due to the influence of these factors, especially tidal/wave erosion, the Na_2CO_3-Si pool in the sediment was smaller than that in the upper slope areas (Fig. 8). Combined with the latest rate of sea level rise around the Bohai Sea (Wang et al., 2019a; Wang et al., 2019b), we estimated that the amorphous Si lost by soil erosion caused by sea level rise at the margin of the BWNR would potentially transport about 3 t Si to the coastal seawater annually. These calculations suggest that this coastal wetland system has the potential to provide amorphous Si to the estuary in the same order of magnitude as medium-size rivers in Tianjin city (Sun, 2022). If these data are applicable to other wetlands that are also subject to margin erosion caused by sea level rise, the coastal wetland systems do not only serve as nursery habitats and storm surge mitigators but also act as an important source of Si. Hence, the coastal wetland systems play a vital role in the biogeochemical Si cycling and the dynamics of phytoplankton communities in estuaries.

5. Conclusion

The total Si in soils and sediments of Beidagang Wetland Nature Reserve consisted of 97%–98% stable Si and 2%–3% labile Si. Within the labile fraction, biogenic amorphous Si was the largest proportion in all profiles. Scanning electron microscopy indicated that phytoliths dominated the biogenic amorphous Si pool in all soil horizons, while diatoms were only observed in the sediments. Significant correlations between soil pH, SOC and total P with different Si fractions suggested that Si fractionations could be affected by soil properties. Although the $CaCl_2$-Si fraction was the smallest component of the labile fraction, it played a central role in the inter-transformation among different Si fractions. Under the influence of soil erosion, the inter-transformation among different Si fractions in the sediments became weakened. With the influences of margin erosion under sea level rise, the storage of non-crystalline Si in sediment was lower than that in soil, indicating that the coastal wetland ecosystems could act an important source of Si for the estuary. Therefore, our findings suggest that the increased DSi could then be utilized partly by diatoms, contributing to coastal primary production to drive estuarine biogeochemical Si cycling. In this regard, under future sea level rise and increased marginal erosion, it is necessary to quantify the labile Si transported from coastal wetlands to the estuaries in future studies. This will provide the scientific basis for unraveling the Si biogeochemical cycling in coastal wetland and optimizing ecosystem management in these regions.

Declaration of Competing Interest

The authors declare that they have no known competing financial interests or personal relationships that could have appeared to influence the work reported in this paper.

Data availability

No data was used for the research described in the article.

Acknowledgments

This research was financially supported by National Natural Science Foundation of China (Grant Nos. 41930862, 42141014 and 42225101) and China Postdoctoral Science Foundation (2021M702426).

Appendix A. Supplementary data

Supplementary data to this article can be found online at https://doi.org/10.1016/j.geoderma.2023.116602.

References

Andreola, F., Castellini, E., Manfredini, T., Romagnoli, M., 2004. The role of sodium hexametaphosphate in the dissolution process of kaolinite and kaolin. J. Eur. Ceram. Soc. 24, 2113–2124. https://doi.org/10.1016/S0955-2219(03)00366-2.

Basile-Doelsch, I., Meunier, J.D., Parron, C., 2005. Another continental pool in the terrestrial silicon cycle. Nature 433, 399–402. https://doi.org/10.1038/nature03217.

Conley, D.J., Sommer, M., Meunier, J.D., Kaczorek, D., Saccone, L., 2006. Silicon in the terrestrial biogeosphere. In: Ittekot, V., Unger, D., Humborg, C., Tac An, N. (Eds.), The Silicon Cycle: Human Perturbations and Impacts on Aquatic Systems. Island Press, Washington, DC, pp. 13–28.

Cornelis, J.T., Delvaux, B., Georg, R.B., Lucas, Y., Ranger, J., Opfergelt, S., 2011. Tracing the origin of dissolved silicon transferred from various soil-plant systems towards rivers: a review. Biogeosciences 8, 89–112. https://doi.org/10.5194/bg-8-89-2011.

Cornelis, J.-T., Delvaux, B., Cooke, J., 2016. Soil processes drive the biological silicon feedback loop. Func. Ecol. 30 (8), 1298–1310.

de Tombeur, F., Turner, B.L., Laliberté, E., Lambers, H., Mahy, G., Faucon, M.P., Zemunik, G., Cornelis, J.T., 2020. Plants sustain the terrestrial silicon cycle during ecosystem retrogression. Science 369 (6508), 1245–1248. https://doi.org/10.1126/science.abc0393.

DeLaune, R.D., White, J.R., 2012. Will coastal wetlands continue to sequester carbon in response to an increase in global sea level?: a case study of the rapidly subsiding Mississippi river deltaic plain. Clim. Change 110, 297–314. https://doi.org/10.1007/s10584-011-0089-6.

Delvaux, B., Li, Z.M., 2023. Silicon and other non-metal elements from Group 14. Reference Module in Earth Systems and Environmental Sciences, Elsevier. https://doi.org/10.1016/B978-0-12-822974-3.00158-0.

Dietzel, M., 2000. Dissolution of silicates and the stability of polysilicic acid. Geochim. Cosmochim. Acta 64, 3275–3281. https://doi.org/10.1016/S0016-7037(00)00426-9.

Dietzel, M., 2002. Interaction of polysilicic and monosilicic acid with mineral surfaces. In: Stober, I., Bucher, K. (Eds.), Water-Rock Interaction. Kluwer Academic Publisher, pp. 207–235. https://doi.org/10.1007/978-94-010-0438-1_9.

Dixit, S., Van Cappellen, P., Van Bennekom, A.J., 2001. Processes controlling solubility of biogenic silica and pore water build-up of silicic acid in marine sediments. Mar. Chem. 73, 333–352. https://doi.org/10.1016/S0304-4203(00)00118-3.

Dove, P.M., Elston, S.F., 1992. Dissolution kinetics of quartz in sodium chloride solutions: analysis of existing data and a rate model for 25°C. Geochim. Cosmochim. Acta 56 (12), 4147–4156. https://doi.org/10.1016/0016-7037(92)90257-J.

Fraysse, F., Pokrovsky, O.S., Schott, J., Meunier, J.D., 2009. Surface chemistry and reactivity of plant phytoliths in aqueous solutions. Chem. Geol. 258, 197–206. https://doi.org/10.1016/j.chemgeo.2008.10.003.

Gallinari, M., Ragueneau, O., Corrin, L., DeMaster, D.J., Treguer, P., 2002. The importance of water column processes on the dissolution properties of biogenic silica in deep-sea sediments I. Solubility. Geochim. Cosmochim. Acta 66, 2701–2717. https://doi.org/10.1016/S0016-7037(02)00874-8.

Gehlen, M., Van Raaphorst, W., 2002. The role of adsorption–desorption surface reactions in controlling interstitial $Si(OH)_4$ concentrations and enhancing $Si(OH)_4$ turn-over in shallow shelf seas. Cont. Shelf Res. 22, 1529–1547. https://doi.org/10.1016/S0278-4343(02)00016-X.

Georgiadis, A., Sauer, D., Herrmann, L., Breuer, J., Zarei, M., Stahr, K., 2013. Development of a method for sequential Si extraction from soils. Geoderma 209, 251–261. https://doi.org/10.1016/j.geoderma.2013.06.023.

Georgiadis, A., Sauer, D., Herrmann, L., Breuer, J., Zarei, M., Stahr, K., 2014. Testing a new method for sequential silicon extraction on soils of a temperate–humid climate. Soil Res. 52, 645–657. https://doi.org/10.1071/SR14016.

Georgiadis, A., Rinklebe, J., Straubinger, M., Rennert, T., 2017. Silicon fractionation in Mollic Fluvisols along the Central Elbe River, Germany. Catena 153, 100–105. https://doi.org/10.1016/j.catena.2017.01.027.

Hao, Q., Ma, N., Song, Z.L., Zhang, X.D., Yang, X., Niazi, N.K., Yu, C., Chen, C., Wang, H., 2022. Soil silicon fractions along karst hillslopes of southwestern China. J. Soils Sediments 22, 1121–1134. https://doi.org/10.1007/s11368-022-03136-9.

Hurd, D.C., Birdwhistell, S., 1983. On producing a more general model for biogenic silica dissolution. Am. J. Sci. 283, 1–28. https://doi.org/10.2475/ajs.283.1.1.

Imtiaz, M., Rizwan, M.S., Mushtaq, M.A., Ashraf, M., Shahzad, S.M., Yousaf, B., Saeed, D. A., Rizwan, M., Nawaz, M.A., Mehmood, S., Tu, S., 2016. Silicon occurrence, uptake, transport and mechanisms of heavy metals, minerals and salinity enhanced tolerance in plants with future prospects: a review. J. Environ. Manage. 183, 521–529. https://doi.org/10.1016/j.jenvman.2016.09.009.

Kirwan, M.L., Megonigal, J.P., 2013. Tidal wetland stability in the face of human impacts and sea-level rise. Nature 504, 53–60. https://doi.org/10.1038/nature12856.

Klotzbücher, T., Treptow, C., Kaiser, K., Klotzbücher, A., Mikutta, R., 2020. Sorption competition with natural organic matter as mechanism controlling silicon mobility in soil. Sci. Rep. 10, 1–11. https://doi.org/10.1038/s41598-020-68042-x.

La, W., Han, X., Liu, C.Q., Ding, H., Liu, M., Sun, F., Li, S., Lang, Y., 2022. Sulfate concentrations affect sulfate reduction pathways and methane consumption in coastal wetlands. Water Res. 217, 118441 https://doi.org/10.1016/j.watres.2022.118441.

Li, Z.M., Guo, F., Cornelis, J.T., Song, Z.L., Wang, X., Delvaux, B., 2020. Combined silicon-phosphorus fertilization affects the biomass and phytolith stock of rice plants. Front. Plant Sci. 11, 67. https://doi.org/10.3389/fpls.2020.00067.

Li, Z.M., Meunier, J.D., Delvaux, B., 2022. Aggregation reduces the release of bioavailable silicon from allophane and phytolith. Geochim. Cosmochim. Acta 325, 87–105. https://doi.org/10.1016/j.gca.2022.03.025.

Li, Z., Meunier, J.D., Delvaux, B., 2023. Goethite affects phytolith dissolution through clay particle aggregation and pH regulation. Geochim. Cosmochim. Acta. 349, 11–22. https://doi.org/10.1016/j.gca.2023.03.021.
Li, Z.M., Song, Z.L., Parr, J.F., Wang, H., 2013. Occluded C in rice phytoliths: implications to biogeochemical carbon sequestration. Plant Soil 370, 615–623. https://doi.org/10.1007/s11104-013-1661-9.
Liang, Y., Nikolic, M., Bélanger, R., Gong, H., Song, A., 2015. Silicon in Agriculture. From Theory to Practice. Springer, Dordrecht. https://doi.org/10.1007/978-94-017-9978-2.
Liu, L., Song, Z.L., Yu, C., Yu, G., Ellam, R.M., Liu, H., Singh, B.P., Wang, H., 2020. Silicon effects on biomass carbon and phytolith-occluded carbon in grasslands under high-salinity conditions. Front. Plant Sci. 11, 657. https://doi.org/10.3389/fpls.2020.00657.
Lu, R., 2000. Methods of Soil and Agrochemical Analysis. China Agricultural Science and Technology Press, Beijing (in Chinese).
Ma, J.F., Yamaji, N., Mitani, N., Tamai, K., Konishi, S., Fujiwara, T., Katsuhara, M., Yano, M., 2007. An efflux transporter of silicon in rice. Nature 448, 209–212. https://doi.org/10.1038/nature05964.
Matichenkov, V.V., Bocharnikova, E.A., 2001. The relationship between silicon and soil physical and chemical properties. In: Datnoff, L.E., Snyder, G.H., Korndörfer, G.H. (Eds.), Silicon in Agriculture. Elsevier Science B.V, Amsterdam, pp. 209–219. https://doi.org/10.1016/S0928-3420(01)80017-3.
Matichenkov, V.V., Snyder, G.H., 1996. The mobile silicon compounds in some South Florida soils. Eurasian Soil Sci. 12, 1165–1180.
Nelson, D.M., Tréguer, P., Brzezinski, M.A., Leynaert, A., Quéguiner, B., 1995. Production and dissolution of biogenic silica in the ocean: revised global estimates, comparison with regional data and relationship to biogenic sedimentation. Global Biogeochem. Cy. 9, 359–372. https://doi.org/10.1029/95GB01070.
Nguyen, M.N., Meharg, A.A., Carey, M., Dultz, S., Marone, F., Cichy, S.B., Tran, C.T., Le, G.H., Mai, N.T., Nguyen, T.T., 2019. Fern, Dicranopteris linearis, derived phytoliths in soil: Morphotypes, solubility and content in relation to soil properties. Eur. J. Soil Sci. 70, 507–517. https://doi.org/10.1111/ejss.12754.
Opfergelt, S., de Bournonville, G., Cardinal, D., André, L., Delstanche, S., Delvaux, B., 2009. Impact of soil weathering degree on silicon isotopic fractionation during adsorption onto iron oxides in basaltic ash soils. Cameroon. Geochim. Cosmochim. Acta 73 (24), 7226–7240.
Parr, J.F., Sullivan, L.A., 2005. Soil carbon sequestration in phytoliths. Soil Biol. Biochem. 37, 117–124. https://doi.org/10.1016/j.soilbio.2004.06.013.
Puppe, D., 2020. Review on protozoic silica and its role in silicon cycling. Geoderma 365, 114224. https://doi.org/10.1016/j.geoderma.2020.114224.
Saccone, L., Conley, D.J., Koning, E., Sauer, D., Sommer, M., Kaczorek, D., Blecker, S.W., Kelly, E.F., 2007. Assessing the extraction and quantification of amorphous silica in soils of forest and grassland ecosystems. Eur. J. Soil Sci. 58, 1446–1459. https://doi.org/10.1111/j.1365-2389.2007.00949.x.
Sapkota, Y., White, J.R., 2020. Carbon offset market methodologies applicable for coastal wetland restoration and conservation in the United States: a review. Sci. Total Environ. 701, 134497 https://doi.org/10.1016/j.scitotenv.2019.134497.
Sartor, L.R., Graham, R.C., Ying, S.C., Andrade, G.R., Montes, C.R., Ferreira, T.O., 2019. Are hypersaline tidal flat soils potential silicon sinks in coastal wetlands? Geoderma 337, 215–224. https://doi.org/10.1016/j.geoderma.2018.08.028.
Sauer, D., Saccone, L., Conley, D.J., Herrmann, L., Sommer, M., 2006. Review of methodologies for extracting plant-available and amorphous Si from soils and aquatic sediments. Biogeochemistry 80, 89–108. https://doi.org/10.1007/s10533-005-5879-3.
Schuerch, M., Spencer, T., Temmerman, S., Kirwan, M.L., Wolff, C., Lincke, D., McOwen, C.J., Pickering, M.D., Reef, R., Vafeidis, A.T., Hinkel, J., Nicholls, R.J., Brown, S., 2018. Future response of global coastal wetlands to sea-level rise. Nature 561, 231–234. https://doi.org/10.1038/s41586-018-0476-5.
Siipola, V., Lehtimäki, M., Tallberg, P., 2016. The effects of anoxia on Si dynamics in sediments. J. Soils Sediments 16, 266–279. https://doi.org/10.1007/s11368-015-1220-5.
Sommer, M., Kaczorek, D., Kuzyakov, Y., Breuer, J., 2006. Silicon pools and fluxes in soils and landscapes—a review. J. Plant Nutr. Soil Sci. 169, 310–3291. https://doi.org/10.1002/jpln.200521981.
Song, Z.L., Wang, H.L., Strong, P.J., Shan, S., 2014. Increase of available soil silicon by Si-rich manure for sustainable rice production. Agron. Sustain. Dev. 34, 813–819. https://doi.org/10.1007/s13593-013-0202-5.
Song, Z.L., McGrouther, K., Wang, H., 2016. Occurrence, turnover and carbon sequestration potential of phytoliths in terrestrial ecosystems. Earth Sci. Rev. 158, 19–30. https://doi.org/10.1016/j.earscirev.2016.04.007.
Song, Z.L., Liu, H., Strömberg, C.A., Wang, H., Strong, P.J., Yang, X., Wu, Y., 2018. Contribution of forests to the carbon sink via biologically-mediated silicate weathering: a case study of China. Sci. Total Environ. 615, 1–8. https://doi.org/10.1016/j.scitotenv.2017.09.253.
Song, Z.L., Wu, Y., Yang, Y., Zhang, X.D., Van Zwieten, L., Bolan, N., Li, Z.M., Liu, H., Hao, Q., Yu, C., Sun, X., Song, A., Wang, W., Liu, C., Wang, H., 2022. High potential of stable carbon sequestration in phytoliths of China's grasslands. Glob. Chang. Biol. 28, 2736–2750. https://doi.org/10.1111/gcb.16092.
Steinmuller, H.E., Hayes, M.P., Hurst, N.R., Sapkota, Y., Cook, R.L., White, J.R., Xue, Z., Chambers, L.G., 2020. Does edge erosion alter coastal wetland soil properties? A multi-method biogeochemical study. Catena 187, 104373. https://doi.org/10.1016/j.catena.2019.104373.
Street-Perrott, F.A., Barker, P.A., 2008. Biogenic silica: a neglected component of the coupled global continental biogeochemical cycles of carbon and silicon. Earth Surf. Proc. Land. 33, 1436–1457. https://doi.org/10.1002/esp.1712.
Struyf, E., Conley, D.J., 2009. Silica: an essential nutrient in wetland biogeochemistry. Front. Ecol. Environ. 7, 88–94. https://doi.org/10.1890/070126.
Struyf, E., Smis, A., Van Damme, S., Garnier, J., Govers, G., Van Wesemael, B., Conley, D. J., Batelaan, O., Frot, E., Clymans, W., Vandevenne, F., Lancelot, C., Goos, P., Meire, P., 2010. Historical land use change has lowered terrestrial silica mobilization. Nat. Commun. 1, 1–7. https://doi.org/10.1038/ncomms1128.
Sun, C., 2022. Composition and transport of carbon and silicon in rivers and wetlands around the Bohai Sea and the budget of silicon and carbon in the Bohai (Master's Thesis). First Institute of Oceanography, Qingdao, China (in Chinese with English abstract).
Tian, H., Chen, G., Zhang, C., Melillo, J.M., Hall, C.A., 2010. Pattern and variation of C: N: P ratios in China's soils: a synthesis of observational data. Biogeochemistry 98, 139–151. https://doi.org/10.1007/s10533-009-9382-0.
Tréguer, P., Bowler, C., Moriceau, B., Dutkiewicz, S., Gehlen, M., Aumont, O., Bittner, L., Dugdale, R., Finkel, Z., Iudicone, D., Jahn, O., Guidi, L., Lasbleiz, M., Leblanc, K., Levy, M., Pondaven, P., 2018. Influence of diatom diversity on the ocean biological carbon pump. Nat. Geosci. 11, 27–37. https://doi.org/10.1038/s41561-017-0028-x.
Tréguer, P.J., Sutton, J.N., Brzezinski, M., Charette, M.A., Devries, T., Dutkiewicz, S., Ehlert, C., Hawkings, J., Leynaert, A., Liu, S.M., Llopis Monferrer, N., López-Acosta, M., Maldonado, M., Rahman, S., Ran, L., Rouxel, O., 2021. Reviews and syntheses: The biogeochemical cycle of silicon in the modern ocean. Biogeosciences 18 (4), 1269–1289.
Van Cappellen, P., Qiu, L., 1997. Biogenic silica dissolution in sediments of the Southern Ocean. II. Kinetics. Deep Sea Res. Part II Top. Stud. Oceanogr. 44, 1129–1149. https://doi.org/10.1016/S0967-0645(96)00112-9.
Vander Linden, C., Li, Z.M., Iserentant, A., Van Ranst, E., de Tombeur, F., Delvaux, B., 2021. Rainfall is the major driver of plant Si availability in perudic gibbsitic Andosols. Geoderma 404, 115295. https://doi.org/10.1016/j.geoderma.2021.115295.
Walkley, A., Black, I.A., 1934. An examination of the Degtjareff method for determining soil organic matter, and a proposed modification of the chromic acid titration method. Soil Sci. 37 (1), 29–38.
Wang, F., Li, J.F., Shi, P.X., Shang, Z.W., Li, Y., Wang, H., 2019a. The impact of sea-level rise on the coast of Tianjin-Hebei, China. China Geology 2, 26–39. https://doi.org/10.31035/cg2018061.
Wang, H., Teng, C., Li, H., Sun, X., Jiang, C., Lou, L., Yue, C., Zhang, Z., 2018. Microbial community shifts trigger loss of orthophosphate in wetland soils subjected to experimental warming. Plant Soil 424, 351–365. https://doi.org/10.1007/s11104-017-3538-9.
Wang, Y., Zhang, B., Jiang, D., Chen, G., 2019b. Silicon improves photosynthetic performance by optimizing thylakoid membrane protein components in rice under drought stress. Environ. Exp. Bot. 158, 117–124. https://doi.org/10.1016/j.envexpbot.2018.11.022.
White, A.F., Vivit, D.V., Schulz, M.S., Bullen, T.D., Evett, R.R., Aagarwal, J., 2012. Biogenic and pedogenic controls on Si distributions and cycling in grasslands of the Santa Cruz soil chronosequence. California. Geochim. Cosmochim. Acta 94, 72–94. https://doi.org/10.1016/j.gca.2012.06.009.
Wu, L.L., Song, Z.L., Yang, X., Zhang, X.D., Hao, Q., Xia, S., Zhao, X., 2022. Variation of soil silicon fractions and bioavailability during centennial-scale evolution of ecosystem after glacier retreat. Soil Sci. Soc. Am. J. 86, 552–565. https://doi.org/10.1002/saj2.20386.
Xia, S.P., Song, Z., Li, Q., Guo, L., Yu, C., Singh, B.P., Fu, X., Chen, C., Wang, Y., Wang, H., 2021a. Distribution, sources, and decomposition of soil organic matter along a salinity gradient in estuarine wetlands characterized by C: N ratio, $^{\delta 1}$3C-$^{\delta 1}$5N, and lignin biomarker. Glob. Chang. Biol. 27, 417–434. https://doi.org/10.1111/gcb.15403.
Xia, S.P., Wang, W.Q., Song, Z.L., Kuzyakov, Y., Guo, L.D., Van Zwieten, L., Li, Q., Hartley, I.P., Yang, Y., Wang, Y., Quine, T.A., Liu, C., Wang, H., 2021b. *Spartina alterniflora* invasion controls organic carbon stocks in coastal marsh and mangrove soils across tropics and subtropics. Glob. Chang. Biol. 27, 1627–1644. https://doi.org/10.1111/gcb.15516.
Xia, S.P., Song, Z.L., Van Zwieten, L., Guo, L.D., Yu, C.X., Wang, W.Q., Li, Q., Hartley, L. P., Yang, Y.H., Liu, H.Y., Wang, Y.D., Ran, X.B., Liu, C.Q., Wang, H.L., 2022. Storage, patterns and influencing factors for soil organic carbon in coastal wetlands of China. Glob. Chang. Biol. 28, 6065–6085. https://doi.org/10.1111/gcb.16325.
Xiao, D., Deng, L., Kim, D.G., Huang, C., Tian, K., 2019. Carbon budgets of wetland ecosystems in China. Glob. Chang. Biol. 25, 2061–2076. https://doi.org/10.1111/gcb.14621.
Yang, S., Hao, Q., Liu, H., Zhang, X.D., Yu, C., Yang, X.M., Xia, S.P., Yang, W., Li, J., Song, Z.L., 2019. Impact of grassland degradation on the distribution and bioavailability of soil silicon: implications for the Si cycle in grasslands. Sci. Total Environ. 657, 811–818. https://doi.org/10.1016/j.scitotenv.2018.12.101.
Yang, X.M., Song, Z.L., Yu, C., Ding, F., 2020a. Quantification of different silicon fractions in broadleaf and conifer forests of northern China and consequent implications for biogeochemical Si cycling. Geoderma 361, 114036. https://doi.org/10.1016/j.geoderma.2019.114036.
Yang, X.M., Song, Z.L., Qin, Z., Wu, L., Yin, L., Van Zwieten, L., Song, A., Ran, X., Yu, C., Wang, H., 2020b. Phytolith-rich straw application and groundwater table management over 36 years affect the soil-plant silicon cycle of a paddy field. Plant Soil 454, 343–358. https://doi.org/10.1007/s11104-020-04656-4.
Yang, X.M., Song, Z.L., Van Zwieten, L., Sun, X., Yu, C., Wang, W., Liu, C., Wang, H., 2021. Spatial distribution of plant-available silicon and its controlling factors in paddy fields of China. Geoderma 401, 115215. https://doi.org/10.1016/j.geoderma.2021.115215.

Yu, X., Li, Y., Xi, M., Kong, F., Pang, M., Yu, Z., 2019. Ecological vulnerability analysis of Beidagang National Park. China. Front. Earth Sci. 13, 385–397. https://doi.org/10.1007/s11707-018-0726-8.

Zhang, X.D., Song, Z.L., Hao, Q., Yu, C.X., Liu, H., Chen, C., Müller, K., Wang, H., 2020. Storage of soil phytoliths and phytolith-occluded carbon along a precipitation gradient in grasslands of northern China. Geoderma 364, 114200. https://doi.org/10.1016/j.geoderma.2020.114200.

Zuo, X., Lu, H., Gu, Z., 2014. Distribution of soil phytolith-occluded carbon in the Chinese Loess Plateau and its implications for silica–carbon cycles. Plant Soil 374, 223–232. https://doi.org/10.1007/s11104-013-1850-6.